

TlBr_xI_{1-x} Photodetectors for Scintillation Spectroscopy

K. S. Shah, J. C. Lund, F. Olschner, J. Zhang, L. P. Moy, M. R. Squillante, W. W. Moses, and S. E. Derenzo

Abstract—This paper reports on the evaluation of photodetectors fabricated from a ternary semiconductor, TlBr_xI_{1-x}, for application in scintillation spectroscopy. These photodetectors are characterized in terms of their resistivity, charge transport parameters, quantum efficiency as a function of wavelength, and finally their performance as scintillation spectrometers. The details about TlBr_xI_{1-x} purification, crystal growth and device fabrication are also addressed.

I. INTRODUCTION

IN recent years, there has been considerable interest in development of high-resolution solid-state photodetectors for use in scintillation spectroscopy [1]–[4]. Solid-state photodetectors show significant advantages over conventional photomultiplier tubes such as increased quantum efficiency at wavelengths corresponding to the scintillator output, smaller size, and insensitivity to magnetic fields. In this paper, we report on the development of solid-state photodetectors fabricated from a new ternary semiconductor, TlBr_xI_{1-x}.

TlBr_xI_{1-x} is a promising photodetector material because its semiconducting bandgap can be changed from 2.1 eV (bandgap (indirect) of TlI) to 2.7 eV (bandgap (indirect) of TlBr) by altering the composition of the ternary crystals. Since all semiconductors show maximum photo-response at photon energies corresponding to their bandgap, the spectral response of the TlBr_xI_{1-x} photodetectors can be tuned (by adjusting composition) to match almost all common inorganic scintillators. In addition, the bandgap of the TlBr_xI_{1-x} crystals is large enough to allow low intrinsic carrier concentration and thus provide low noise performance. Also, the physical properties of this ternary material are amenable to relatively easy and rapid purification and crystal growth procedures. TlBr_xI_{1-x} has a CsCl-type simple cubic crystal structure (for $x > 0.3$), and good-quality crystals can be grown directly from the melt in this composition range [5]. Finally, TlBr_xI_{1-x}

crystals are relatively hard with a Knoop hardness number of 40, while TlBr is softer with a Knoop hardness number of 12 [6]. This is important from the viewpoint of device processing, because soft semiconductors require more delicate handling techniques and often suffer from fabrication-induced defects.

In view of these attractive properties, we have been investigating TlBr_xI_{1-x} as a photodetector material. This investigation covered purification of TlBr and TlI starting materials, crystal growth of TlBr_xI_{1-x}, and the fabrication and characterization of TlBr_xI_{1-x} photodetectors.

II. PREPARATION OF TlBr_xI_{1-x} CRYSTALS

Extensive purification was carried out of the starting materials (TlBr and TlI) prior to the crystal growth process. Commercially available TlBr and TlI (Æsar-99.999%) powders were sealed in an evacuated ampoule and were purified by multiple pass zone refining in a two-zone horizontal furnace [7], [8]. About 50 zone refining passes were carried out, and the impurities in the starting material were found to travel with the liquid zone (due to segregation process) and accumulate at one end of the ampoule, leaving the other end considerably purer. A section of the ingot from the pure end was then removed and was used for crystal growth experiments.

The choice of the crystal growth process to be used for producing TlBr_xI_{1-x} crystals was made on the basis of the phase diagram of the TlBr-TlI system which is shown in Fig. 1 [9], [10]. As can be seen in the phase diagram, for most of the composition range ($x > 0.3$), the ternary compound shows no solid-solid phase change. Hence, high-quality crystals of the ternary compound (of cubic crystal structure, with $x > 0.3$) can be grown directly from the melt, and the Bridgman technique was used to grow the TlBr_xI_{1-x} crystals [11].

During the Bridgman crystal growth experiments, purified TlBr and TlI were loaded into a clean quartz ampoule (14 mm i.d. and 19 mm o.d.) in amounts determined by the required crystal composition, and the ampoule was evacuated and sealed under an argon pressure of 50 μm (Hg). The ampoule was then placed in a vertical tube furnace, the temperature of which was controlled at 550°C. This temperature being higher than the melting point of both the starting materials caused TlBr and TlI to react in the molten state and form TlBr_xI_{1-x}. The ampoule was dropped through the furnace at a rate of 5 mm/day, and crystallization occurred as the ampoule reached the bot-

Manuscript received May 17, 1994; revised July 18, 1994. This work was supported in part by the U.S. Department of Energy under Contracts DE-AC01-89ER80B20 and DE-AC03-76SF00098, in part by the U.S. National Institute of Health Contract IR43CA53082-01, in part by Public Health Service Grant P01 25840 and R01 CA48002, and in part by a grant from the Whitaker Foundation.

K. S. Shah, J. C. Lund, F. Olschner, J. Zhang, L. P. Moy, and M. R. Squillante are with Radiation Monitoring Devices, Inc., Waretown, MA 02172.

W. W. Moses and S. E. Derenzo are with Lawrence Berkely Laboratory, University of California, Berkeley, CA 94720.

IEEE Log Number 9405294.

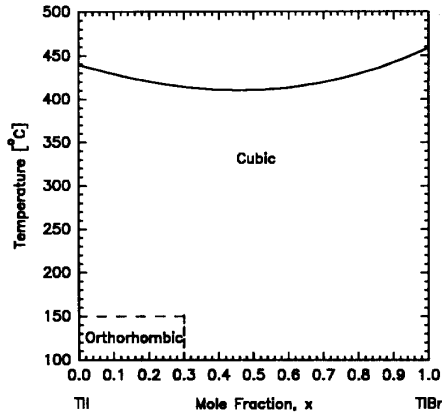


Fig. 1. Phase diagram of the TlBr-TlI system. This phase diagram was prepared from the data published in [9].

tom of the furnace due to sharp temperature gradient at that point. The composition of the growing crystal was the same as the composition of the melt because the solidus and the liquidus lines overlap each other in the TlI-TlBr phase diagram [10].

TlBr_xI_{1-x} crystals of three compositions ($x = 0.35, 0.5, 1.0$) were grown in this manner. These crystals were transparent, and changed from bright red (for $x = 0.35$) to light yellow (for $x = 1$).

III. CHARACTERIZATION OF TlBr_xI_{1-x} CRYSTALS

The Bridgman-grown TlBr_xI_{1-x} crystals were characterized by measuring their optical as well as electrical properties. The optical characterization involved measurement of the optical transmission characteristics of the TlBr_xI_{1-x} crystals using a Bausch and Lomb monochromator (#2D126). These transmission characteristics are shown in Fig. 2. These measurements were important because they enabled us to establish the relationship between the semiconducting bandgap and the crystal composition for the TlBr_xI_{1-x} system (see Fig. 3).

The electrical characterization of the TlBr_xI_{1-x} crystals involved measurement of their resistivity and their charge transport properties. The resistivity measurements were made by depositing carbon electrodes on both sides of TlBr_xI_{1-x} crystal slices and recording current-voltage behavior of these devices. The $I(V)$ behavior was reasonably linear, and we were able to estimate the resistivity of the crystals from these data ($\rho_{x=0.35} = 3 \times 10^{10} \Omega \text{ cm}$, $\rho_{x=0.5} = 9 \times 10^9 \Omega \text{ cm}$, $\rho_{x=1} = 5 \times 10^{11} \Omega \text{ cm}$). The mobility lifetime product of electrons ($\mu\tau$)_e in TlBr_xI_{1-x} was estimated by irradiating the TlBr_xI_{1-x} crystals with an ²⁴¹Am source (60 keV γ -rays) and measuring the resulting spectra on a calibrated energy scale. From these measurements, the mobility lifetime product of electrons in TlBr_xI_{1-x} was computed ($\mu\tau_{x=0.35} = 1 \times 10^{-5} \text{ cm}^2/\text{V}$ and $\mu\tau_{x=1} = 2 \times 10^{-5} \text{ cm}^2/\text{V}$) using the method developed by Mayer [12].

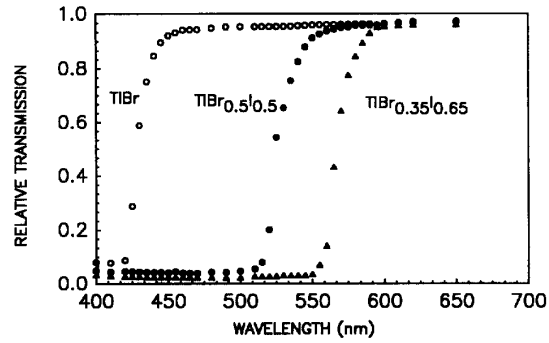


Fig. 2. Relative optical transmission as a function of the wavelength of the incident light for three compositions of the TlBr_xI_{1-x} crystals. The band edge is clearly visible in each transmission curve, and the band edge energy decreased with decreasing bromine concentration.

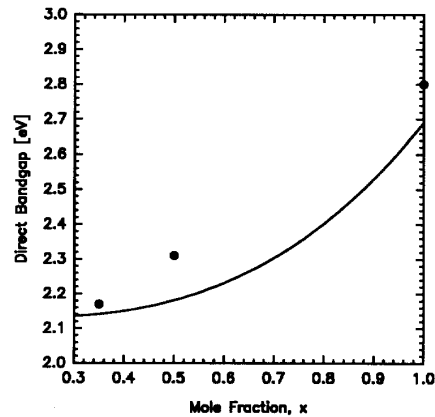


Fig. 3. Bandgap energy versus composition for TlBr_xI_{1-x} crystals. The solid line is from [9] and the solid circles are based on our experimental measurements.

IV. TlBr_xI_{1-x} PHOTODETECTOR STUDIES

A. Photodetector Fabrication

In order to fabricate TlBr_xI_{1-x} photodetectors, the cylindrical Bridgman-grown crystals were cut into wafers about 500 μm thick using a wire saw. These wafers were lapped and polished using Al₂O₃ grit (5 and 1 μm , respectively) and then etched using a 10% bromine in methanol solution. The resulting slices were clear and had a good surface finish. Transparent, conductive front electrodes were deposited on such wafers. We experimented with a variety of materials such as phosphoric acid solution, thin evaporated films of gold (100 \AA thick), and thin sheets of conducting hydrogels (RG-42, RG-72—manufactured by Promcon, a division of Medtronic Inc.) in order to fabricate suitable front contacts. Best results (in terms of photodetector performance) were obtained using phosphoric acid solution. The back electrodes were fabricated by painting a carbon suspension (Eccocoat, Emerson and Cummings Inc., #256) on the crystal surface. Thin palladium wires were attached to front as well as back contacts, and the devices were finally secured on ceramic substrates using a silicone-based adhesive (Dow

Corning, RTV 3140). These devices were then characterized by measuring their quantum efficiency at different wavelengths as well as their performance as scintillation spectrometers.

B. Measurement of Quantum Efficiency

The quantum efficiency of the $\text{TlBr}_x\text{I}_{1-x}$ photodetectors was measured by illuminating the photodetectors with a calibrated Bausch and Lomb monochromator (#2D126) and measuring the resulting photocurrent in the detector with an electrometer (Keithley, #614). The measured detector response was then normalized with respect to its area in order to compute the variation in the quantum efficiency of the $\text{TlBr}_x\text{I}_{1-x}$ photodetectors with the incident optical wavelength. Fig. 4 shows such a quantum efficiency versus wavelength behavior for a $\text{TlBr}_{0.35}\text{I}_{0.65}$ photodetector.

As expected, the photodetector showed high quantum efficiency for optical photons with energy greater than its bandgap ($hm > 2.2$ eV, or $k < 570$ nm). As seen in Fig. 4, the photodetectors showed a relatively broad spectral response due to the indirect bandgap structure of the $\text{TlBr}_x\text{I}_{1-x}$ crystals. Also, the quantum efficiency decreased as the energy of the optical photons increased. Such a behavior in case of other photodetectors has been explained by considering the presence of a damaged surface layer (or a “dead layer”) under the front contact where the transport parameters are considerably worse than in the bulk material [13]. As the photon energy increases, the optical photons do not penetrate deep into the crystal, and almost all excess carriers are generated just underneath the front contact (in the dead layer). Since these carriers are not collected effectively due to poor transport properties in the dead layer, the quantum efficiency is low for these photon wavelengths. Thus, the quantum efficiency of the $\text{TlBr}_x\text{I}_{1-x}$ photodetectors can be increased by improving the quality of the crystals used for photodetector fabrication and thereby reducing the dead layer thickness.

Photodetectors fabricated from ternary crystals with other compositions were found to exhibit similar behavior, but the peak response was shifted in accordance with the bandgap for the particular crystal composition. TlBr photodetectors were found to have a relatively narrow spectral response which could be due to a thicker dead layer on the TlBr crystal surface since TlBr crystals are softer as compared to $\text{TlBr}_x\text{I}_{1-x}$ crystals.

C. Evaluation as Scintillation Spectrometers

Next, the $\text{TlBr}_{0.35}\text{I}_{0.65}$ photodetectors were tested as scintillation spectrometers. Since the quantum efficiency of these detectors was high in the 450–600 nm region, the detectors were coupled to a $\text{CsI}(\text{Tl})$ scintillator which shows highest light output amongst all inorganic scintillators (52 000 photons/MeV) and has high output in the wavelength region of 450–600 nm ($k_{\text{max}} = 540$ nm).

The $\text{TlBr}_{0.35}\text{I}_{0.65}$ photodetectors were mounted in a test jig and connected to a low noise preamplifier (Canberra

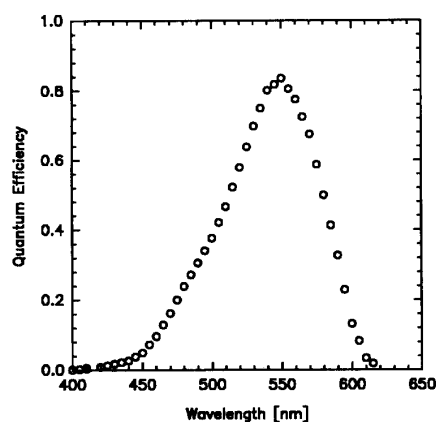


Fig. 4. Relative quantum efficiency of a $\text{TlBr}_{0.35}\text{I}_{0.65}$ photodetector as a function of wavelength of the incident light.

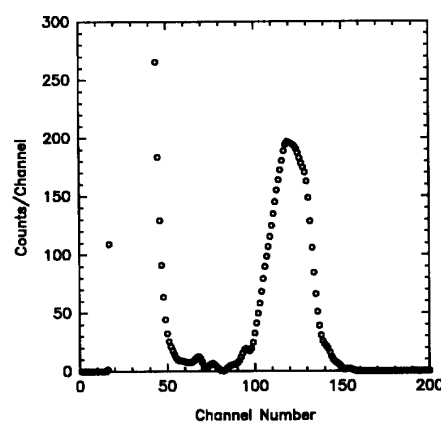


Fig. 5. Pulse height spectrum obtained by irradiating a $\text{TlBr}_{0.35}\text{I}_{0.65}$ photodetector (0.4 cm^2 area, $200 \mu\text{m}$ thick) coupled to a $\text{CsI}(\text{Tl})$ scintillator (5 mm diameter) with 5.5 MeV α -particles (^{241}Am source). The photodetector was operating at room temperature.

#2003). A Canberra spectroscopy amplifier (#2020) was used with a shaping time set to $5 \mu\text{s}$. The spectra were recorded on a Nucleus PCA-1000 residing in an IBM compatible personal computer. Fig. 5 shows an ^{241}Am spectrum (5.5 MeV α -particles) recorded with a $\text{TlBr}_{0.35}\text{I}_{0.65}$ photodetector (0.4 cm^2 area, $200 \mu\text{m}$ thick, with 50 pF capacitance) coupled to a $\text{CsI}(\text{Tl})$ scintillator (5 mm diameter). The detector was operated at 20 V and its performance was limited by the shot noise generated due to the leakage current flowing through the detector. This leakage current (22 nA) is the result of the applied electric field (1000 V/cm) across the detector (having resistivity of $2 \times 10^{10} \text{ cm}$) and was not the result of surface leakage effects.

Finally, a TlBr photodetector ($100 \mu\text{m}$ thick, 0.16 cm^2 area) was also tested as scintillation spectrometer by coupling its transparent front contact to a BGO scintillator (3 mm^3). The photodetector was connected to a low noise, charge sensitive preamplifier (described previously

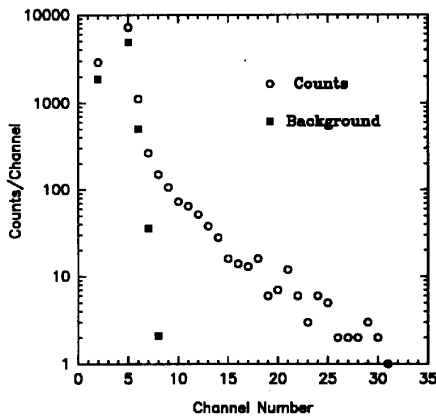


Fig. 6. Pulse height spectrum obtained by irradiating a TlBr photodetector (0.16 cm^2 area, $100 \text{ }\mu\text{m}$ thick) coupled to a BGO scintillator (3 mm^3) with 511 keV photons (^{68}Ge source). The photodetector (along with the scintillator and the charge sensitive preamplifier) was operating at -25°C . Also shown in the figure is the background spectrum acquired under identical test conditions but without irradiation with the ^{68}Ge source.

in [2]), and the preamplifier output was further amplified with a Tennelec TC-222 amplifier operating with a $15 \text{ }\mu\text{s}$ shaping time. The amplifier output was then digitized, and the resulting pulse height spectrum was acquired with a LeCroy 3512 ADC. The photodetector, BGO crystal, and preamplifier assembly was placed in an insulated, temperature controlled chamber. The chamber was flushed with dry nitrogen and then cooled to -25°C . The photodetector was biased at 25 V and the test setup was pulsed with a 1 pC of input charge (6240 electrons). From the resulting spectrum, the system noise was computed to be 535 electrons (FWHM). The test pulse was then removed and the background spectrum shown in Fig. 6 was obtained. The BGO crystal was then irradiated with 511 keV photons (^{68}Ge source) and the resulting pulse height spectrum is also shown in Fig. 6. While the 511 keV photopeak is not visible, there is a clear signal above the background level.

V. SUMMARY

$\text{TlBr}_x\text{I}_{1-x}$ has been investigated as a material for fabrication photodetectors which can be used in scintillation spectroscopy. High-quality crystals of the ternary compound with different compositions were grown by the Bridgman process using purified starting materials. These

crystals were characterized by measuring their electrical and optical properties. From the optical transmission measurements, the relationship between the semiconducting bandgap and the composition of the $\text{TlBr}_x\text{I}_{1-x}$ crystals was established. Photodetectors fabricated from these crystals were found to show relatively broad quantum efficiency-wavelength relation due to the indirect band structure in $\text{TlBr}_x\text{I}_{1-x}$ crystals. Preliminary testing of these photodetectors as scintillation spectrometers was carried out, and the principal factor limiting their performance was found to be the relatively low resistivity of the $\text{TlBr}_x\text{I}_{1-x}$ crystals. In their present form, the $\text{TlBr}_x\text{I}_{1-x}$ photodetectors do not perform as well as the conventional silicon p-i-n photodiodes, especially in terms of the quantum efficiency. However, we believe that improvement in the photodetector performance can be made possible by further enhancing the purity of the starting materials, thereby increasing the resistivity of $\text{TlBr}_x\text{I}_{1-x}$ crystals, and by utilizing improved surface preparation techniques in order to reduce the thickness of the dead layer.

REFERENCES

- [1] R. Farrell, F. Olschner, E. Fredrick, L. McConchie, K. Vanderpuye, M. R. Squillante, and G. Entine, "Large area silicon avalanche photodiodes for scintillation detectors," *Nucl. Inst. Meth.*, vol. A288, p. 137, 1990.
- [2] S. E. Derenzo, W. W. Moses, H. G. Jackson, B. T. Turko, J. L. Cahoon, A. B. Geyer, and T. Vuletich, "Initial characterization of a position sensitive photodiode/BGO detector for PET," *IEEE Trans. Nucl. Sci.*, vol. NS-36, p. 1084, 1989.
- [3] J. M. Markakis, "Mercuric iodide photodetector-cesium iodide scintillator gamma ray spectrometers," *IEEE Trans. Nucl. Sci.*, vol. NS-35, p. 356, 1988.
- [4] D. E. Groom, "Silicon photodiode detection of bismuth germanate scintillation light," *Nucl. Inst. Meth.*, vol. 219, p. 141, 1984.
- [5] K. H. Hellwege, and O. Madelung, Eds., *Landolt-Bornstein Numerical Data and Functional Relationships in Science and Technology*, vol. 17f. New York: Springer-Verlag, 1983.
- [6] J. H. Moore, C. C. Davis, and M. A. Coplan, *Building Scientific Apparatus*, 2nd ed. Reading, MA: Addison-Wesley, 1989.
- [7] W. G. Pfann, *Zone Melting*. New York: Krieger, 1978.
- [8] J. C. Lund, K. S. Shah, M. R. Squillante, L. P. Moy, F. Sinclair, and G. Entine, "Properties of lead iodide semiconductor radiation detectors," *Nucl. Inst. Meth.*, vol. A283, p. 299, 1989.
- [9] M. Ikedo, M. Watari, F. Tateisha, and H. Ishiwatari, "Preparation and characteristics of the TlBr-TlI fiber for a high power CO_2 laser beam," *J. Appl. Phys.*, vol. 60, p. 3035, 1986.
- [10] E. M. Levin, C.R. Robins, and H.F. McMurdie, *Phase Diagrams for Ceramists*, Vol. 1. American Ceramic Society, 1964.
- [11] J. C. Brice, *Crystal Growth Processes*. London: Blackie Halsted Press, 1986.
- [12] J. W. Mayer, "Evaluation of CdTe by nuclear particle measurements," *J. Appl. Phys.*, vol. 38, p. 296, 1967.
- [13] J. Lindmayer and C. Y. Wrigley, *Fundamentals of Semiconductor Devices*. Princeton, NJ: Van Nostrand, 1965, p. 383.